
Perception of inert particles by calanoid copepods: behavioral observations and a numerical model

Marie H. Bundy^{1,4}, Thomas F. Gross², Henry A. Vanderploeg¹ and J. Rudi Strickler³

¹Great Lakes Environmental Research Laboratory, 2205 Commonwealth Blvd, Ann Arbor, MI 48105, ²Skidaway Institute of Oceanography, 10 Ocean Science Circle, Savannah, GA 31411 and ³Center for Great Lakes Studies, University of Milwaukee-Wisconsin, Milwaukee, WI, USA

⁴Present address: Academy of Natural Sciences Estuarine Research Center, 10545 Mackall Road, St Leonard, MD 20685, USA

Abstract. High-resolution video showed freely swimming *Diaptomus sicilis* attacking and capturing inert 50 μm polystyrene beads that were outside the influence of the copepod feeding current. The beads were frequently more than half a body length away and were attacked after the 'bow wake' of the moving copepod displaced the bead away from the copepod. To investigate the hypothesis that deformation of streamlines around the copepod and its first antennae stimulated the attack response, a finite element numerical model was constructed. The model described the fluid interactions between a large object approaching a smaller object in a laminar flow at Reynolds number 5, which is characteristic of the fluid regime experienced by foraging copepods. The model revealed that fluid velocity fluctuations and streamline deformations arose in the region between the two objects as separation distance between the objects decreased. The video observations and the model results support the hypotheses that chemoreception is not required for the detection and capture of large phytoplankton cells [Vanderploeg *et al.*, in Hughes, R.N. (ed.), *Behavioral Mechanisms of Food Selection*. NATO ASI Series G20, 1990; DeMott and Watson, *J. Plankton Res.*, **13**, 1203–1222, 1991], and that swimming behavior plays an integral role in prey detection.

Introduction

Evidence that copepods can detect the presence and position of remotely located prey has been accumulating since 1980, when high-speed cinematography was first used to observe copepod feeding (Alcaraz *et al.*, 1980). However, little is known about either the physical mechanisms or the sensory modalities involved in this process. Calanoid copepods feed on suspended particles at rates that may depend on the olfactory and gustatory qualities, and on nutritional, size and/or movement characteristics of the particles, rather than on particle abundance alone (Harvey, 1937; Donaghay and Small, 1979; Butler *et al.*, 1989; Vanderploeg *et al.*, 1990; DeMott and Watson, 1991). Tethered calanoid adults and juveniles can actively capture non-motile phytoplankton cells entrained in the feeding current by using one or more feeding appendages to direct individual particles to the mouth (Koehl and Strickler, 1981; Paffenhöfer *et al.*, 1982; Vanderploeg and Paffenhöfer, 1985; Paffenhöfer and Lewis, 1990). Large ($>14 \mu\text{m}$) beads may be captured in the same way (Vanderploeg *et al.*, 1990). Both active captures and attacks (an attack is characterized by a jump toward the particle, followed by an active capture) may be executed before the particle contacts a feeding appendage, indicating that some signal regarding particle location is detected by the copepod. Traditionally, the feeding current has been considered as the

vehicle that conveys both chemical (Andrews, 1983) and mechanical (Légier-Visser *et al.*, 1986) signals to the copepod when the copepod is feeding on non-motile prey.

Selection and detection of prey may, however, be two separate processes. DeMott and Watson (1991) used high background levels of chemostimulatory compounds to mask chemical signals from large algal cells, and found that clearance rates and selectivity of *Diaptomus birgei* on large algae were unchanged. These results, coupled with visual observations of tethered copepods showing active capture of inert beads in the feeding current (Vanderploeg *et al.*, 1990), suggest that diaptomids primarily use mechanoreception to detect large particles. The signal most likely originates from the motion of the bead relative to the copepod, as the bead is entrained in the feeding current. Visual observations designed to examine the behavioral processes involved in prey discrimination reveal that the process of selecting for or against ingestion of different particles often occurs after the particle is captured and handled (Paffenhöfer *et al.*, 1982; Cowles *et al.*, 1988; Vanderploeg *et al.*, 1990). The copepod presumably uses mechanoreceptive and chemoreceptive sensilla on the mouthparts (Friedman, 1980) to distinguish particle quality, and then actively rejects unwanted particles.

This study presents the first evidence that free-swimming calanoid copepods attack non-motile inert particles located outside the influence of the feeding current. Freely swimming copepods were observed swimming toward an inert particle, then jumping forward and capturing it. Immediately before the capture event, the particle was displaced away from and in front of the approaching copepod. Here, we used high-resolution video observations to document the attacks and to investigate the hypothesis that the stimulus initiating attack behavior originates as a distortion of the boundary layer around the moving copepod. A numerical model was then used to determine whether a stationary particle in the path of a moving object can cause a distortion of the boundary layer around that object at the Reynolds number (Re) characteristic of the copepod–bead interactions documented by visual observations. The goal of the model was to describe how a copepod may use mechanoreception to detect streamline deformations around its first antennae when the boundary layer around the moving animal interacts with an inert particle in its path. Our results suggest that: (i) mechanoreception is involved in the detection and capture of large non-motile particles; (ii) perception of dissolved chemical cues is not required for the detection and capture of large particles by copepod predators; and (iii) the feeding current is not always involved in the detection and capture of non-motile prey.

Method

Video procedures and behavioral analyses

Diaptomus sicilis females were collected from vertical tows in eastern Lake Michigan using an opening/closing net (202 μm mesh size with a 1 l solid cod-end)

at a 100-m-deep station located 15 km west of Muskegon, Michigan. The ascending net was closed at ~5 m below the thermocline to reduce mechanical damage to the copepods. The contents of the net cod-end were gently poured into 10 l insulated jugs containing water collected from a similar depth as the net tows. Copepods were returned to an environmental room at the Great Lakes Environmental Research Laboratory (GLERL), where they were maintained at 8–10°C and a 12:12 h light:dark cycle. Using a wide-bore glass tube, ~50 *D.sicilis* females and 3–4 males were individually pipetted into 1800 ml of 0.2 µm filtered lake water (FLW), containing ~0.3 mm³ l⁻¹ (360 cells ml⁻¹) *Cryptomonas reflexa* [12 µm equivalent spherical diameter (ESD)]. Copepods were videotaped after at least 48 h acclimation to laboratory conditions.

Twenty-four hours prior to videotaping, ~15 female *D.sicilis* were individually pipetted into a beaker (the 'acclimation vessel') containing 1800 ml FLW to which ~0.3 mm³ l⁻¹ *C.reflexa* and 3–6 ml⁻¹ 50 µm polystyrene beads (specific gravity 1.05 g cm⁻³; Duke Scientific Corp., Palo Alto, CA) had been added. The beads had been repeatedly rinsed in deionized water, centrifuged and resuspended in deionized water. On the day of filming, a 3 l cubic Plexiglas container with a removable lid ('filming vessel') was filled with 2000 ml of FLW and 800 ml water from the acclimation vessel that was first screened through a 10 µm mesh. Adding screened water from the acclimation vessel seemed to reduce the incidence of rapid jumping by the copepods, noted when only FLW was used. Enough algae and beads were then added to create a suspension consisting of 0.2 mm³ l⁻¹ *C.reflexa* and 3–6 ml⁻¹ 50 µm polystyrene beads.

The video system at GLERL, similar to that used by Bundy and Paffenhöfer (1996), consists of a video camera equipped with a near-infrared collimated laser light source and mounted on a three-dimensional motor drive. It is located in the same room in which the copepods were maintained and acclimated. The room was illuminated by dim, diffuse light from cool white fluorescent bulbs. The camera optical set-up utilizes Schlieren optics and resembles that described by Strickler (1985). The database of camera position was synchronized with the video record through a time-code generator and a time-stamp overlay on each video field. In this study, a record of camera position was collected at a sampling rate of either 8 or 15 Hz. The temporal resolution of the video images was 60 Hz. The area of the video camera field of view was 5.75 × 7.50 mm, with spatial resolution of ~10 µm in the plane of view and a depth of field of ~200 µm in the plane of focus. Joysticks and a video monitor in an adjoining room allowed individual copepods to be followed for hours, if necessary, as they moved about in the 3 l filming vessel. Videotaping of copepod-bead interactions was conducted within 10 days of zooplankton collection.

The filming vessel was gently stirred 15 min prior to videotaping to resuspend beads and phytoplankton. One to three copepods were then added to the filming vessel and a single copepod was videotaped for 30–60 min. After an individual had been videotaped, it was removed from the filming vessel and placed in a small beaker. The filming vessel was again gently stirred and another copepod was videotaped after a 15 min period to allow water motion in the filming vessel to dissipate. All copepods were actively swimming at least 48 h after filming, and

each experimental copepod was microscopically examined for broken appendages and measured.

To determine the position and velocities of the beads and the copepod, the coordinates of the copepod's left and right first antennae (A1), the eye, the base and tip of the urosome, along with any particles of interest in the field of view (Figure 1), were digitized in successive video fields using a motion-analysis system (Peak Performance Technologies, Inc.). Two-dimensional data representing points in the camera plane of view were used to calculate swimming trajectories and velocities. Each set of coordinates representing bead location was subjected to a low-pass digital filter to remove high frequencies associated with digitizing error (Weiss *et al.*, 1986). Position data were then mathematically corrected for the movement of the camera. The horizontal and vertical planes of reference were the horizontal and vertical planes of the filming vessel, which were normal to the optical axis.

We examined copepod swimming behavior at a fine temporal scale (60 Hz) immediately before an attack to characterize fully the orientation and trajectory of the copepod body before the attack occurred, and as a means of detecting behavioral responses to the bead. We digitized the position of the copepod body and the bead during an interval beginning after the jump prior to the attack leap (called 'the time interval before capture'). We then determined the orientation of the copepod to the bead, its swimming velocity, and the distance to the bead when the attack occurred (Table I). To investigate the role of body orientation in the remote detection of the bead, we also examined the position and orientation

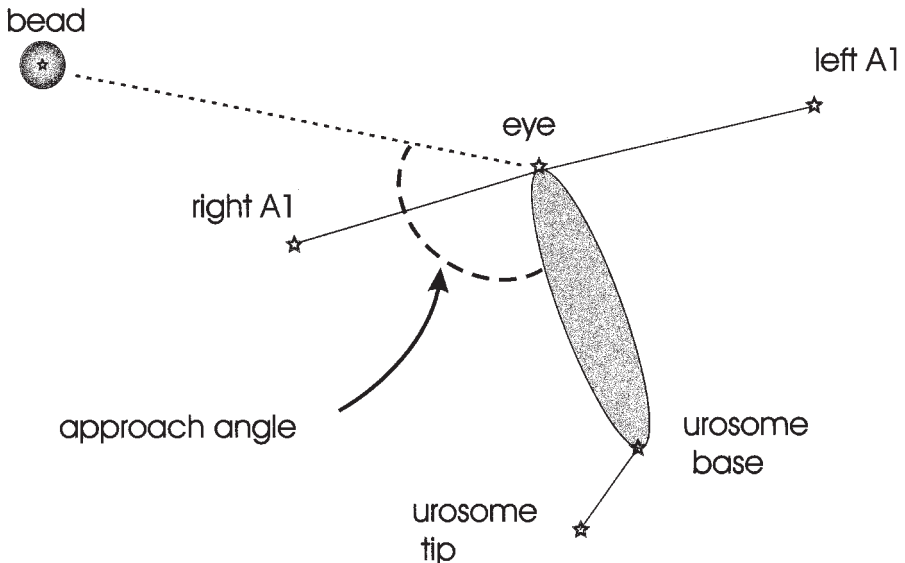


Fig. 1. Schematic drawing of a bead and copepod (not to scale). Stars indicate points digitized in behavioral analyses. The approach angle is defined as the angle composed of the copepod body axis and the trajectory to the bead.

of putative mechanosensory setae on the A1 by using laser scanning confocal microscopy (LSCM) to obtain a three-dimensional image [see Bundy and Paffenhöfer (1993) for methodology].

We also analyzed swimming behavior for 10 s before the attack by digitizing the position of the copepod at 67 ms intervals (15 Hz) (Table II). We calculated

Table I. Behavior of six copepods during the time interval immediately before attack events. Letters indicate different attack events for the same copepod. Sampling frequency = 60 Hz

Copepod	Capture event	Interval before capture (s)	Orientation angle (degrees)		Distance from copepod when bead first moves (mm)	Copepod distance from bead at time of attack (mm)
			After jump	Prior to attack		
1	a	3.10	111	86	1.76	1.08
2	a	0.60	105	89	0.97	a
3	a	1.25	102	89	1.45	1.40 ^b
4	a	0.70	117	90	1.10	0.48
	b	0.07	73	94	1.86	1.39
	c	0.40	106	91	1.57	0.78
5	a	5.00	125	107	1.32	0.93
	b	9.00	107	91	2.10	1.41
6	a	1.10	119	93	1.43	0.48
	b	1.40	113	95	1.76	1.31

^aCopepod used feeding current to capture the bead (see the text for further information).

^bVentral view of copepod (see the text for further explanation).

Table II. Behavior of six copepods during 10 s intervals before attack events. Letters indicate different attack events for the same copepod. Swim interval is the interval between jumps. Swim velocity is the average velocity during each swim interval. Jump velocity is the maximum velocity for each jump. Sampling frequency = 15 Hz

Copepod	Capture event	Swim interval (s)	Swim velocity (mm s ⁻¹)	Jump velocity (mm s ⁻¹)
		Mean ± SD	Mean ± SD	Mean ± SD
1	a	2.10 ± 0.9 (n = 2)	1.13 ± 0.5	19.66 ± 4.4 (n = 3)
2	a	1.84 ± 1.4 (n = 4)	1.10 ± 0.7	13.76 ± 8.2 (n = 5)
3	a	0.98 ± 0.6 (n = 8)	1.87 ± 1.2	22.97 ± 16.1 (n = 9)
4	a	1.43 ± 0.7 (n = 5)	1.31 ± 0.9	28.8 ± 15.5 (n = 6)
	b	0.91 ± 0.5 (n = 8)	1.11 ± 0.7	22.37 ± 12.9 (n = 9)
	c	1.43 ± 1.0 (n = 4)	1.15 ± 0.7	34.39 ± 7.0 (n = 5)
5	a	3.48 ± 1.6 (n = 2)	0.86 ± 0.6	16.05 ± 6.0 (n = 3)
	b	9.00 (n = 1)	1.12 ± 0.7	19.25 ± 7.0 (n = 2)
6	a	1.23 ± 0.7 (n = 6)	1.22 ± 0.8	26.10 ± 5.2 (n = 5)
	b	2.25 ± 0.9 (n = 4)	0.86 ± 0.7	19.16 ± 12.1 (n = 5)

the swimming interval (i.e. the amount of time spent swimming between each jump), jump velocity and swimming velocity from copepod displacement.

A 9 s subset of the 10 s behavioral series (digitized at 67 ms intervals) was subdivided into three 3 s intervals (Table III). The behavior of the copepod during the 3 s immediately before an attack was compared to that during the 3 s intervals beginning 9 and 6 s before an attack. For each 3 s interval, we calculated the copepod movement trajectory, the mean swimming velocity between jumps, and the mean jump velocity. Following the methods of Cain (1989), the swimming trajectory was defined as the direction of movement between each digitized position, with 0° indicating no change in direction between two successive positions. The direction of movement (θ) is defined as a vector with unit length, whose coordinates can be averaged to calculate the mean and the angular deviation of the trajectories. Upward jumps were defined as positive and downward jumps were defined as negative. A runs test (e.g. Dixon and Massey, 1951) was then used to determine whether jumps in any interval were non-randomly directed.

Numerical model

The finite element numerical model used in this study solved for a two-dimensional flow field around two circular cylinders: one cylinder was stationary and the other was embedded in the upstream flow and moving with the streamline velocity. This scenario is physically identical to one where a large moving cylinder approaches a stationary smaller cylinder. The numerical model was based on the assumption that the wake flow and boundary layer constitute the deformed velocity streamlines around the moving copepod. The bead can be considered as an incompressible obstacle, embedded within the wake flow, that further deforms the velocity streamlines. The finite element method allows a grid to resolve the boundaries of the objects in the flow with arbitrary geometry. The goal of this exercise was to examine the hydrodynamics of the simple two-dimensional case of circular cylinders normal to the flow, and to characterize fluid velocities and the geometry of the flow field in the region between the two objects. We suspected that deformation of streamlines around the copepod's first antennae and its mechanoreceptors was the stimulus that initiated attack responses from the copepod, and that these deformations arose when the boundary layer associated with the moving copepod impacted the solid bead. We use the simple case of two cylinders as a test for investigating the potential for flow field distortions to arise between two objects moving relative to each other at low *Re*. The geometry of the copepod antennae approaching a prey item is more like a cylinder moving relative to a sphere. In this case, the magnitude of fluid distortion would most likely be lower and have a different spatial distribution than in the case of two cylinders.

The model solved the vorticity equation with non-linear advection and viscous diffusion terms, and a streamline equation to satisfy the incompressibility requirement. To solve for the flow field, the low-*Re* Navier–Stokes equations were written for two-dimensional flow:

Table III. Behavior of six copepods during 3 s sequential intervals beginning 9 s before attack events. Letters indicate different attack events for the same copepod. Swim trajectory is the change in direction between sequential digitized positions (see the text). Swim velocity is calculated from displacement at each sequential digitized position. Jump velocity is the maximum velocity for each jump. Sampling frequency = 15 Hz

Copepod	event	Swim trajectory (degrees)			Swim velocity (mm s ⁻¹)			Jump velocity (mm s ⁻¹)		
		9–6 s prior Mean ± SD	6–3 s prior Mean ± SD	3 s prior Mean ± SD	9–6 s prior Mean ± SD	6–3 s prior Mean ± SD	3 s prior Mean ± SD	9–6 s prior Mean ± SD	6–3 s prior Mean ± SD	3 s prior Mean ± SD
1	a	80.8 ± 17	42.4 ± 51	35.5 ± 41	1.06 ± 0.3	1.24 ± 0.6	1.1 ± 0.6	–	22.13 ± 1.5 <i>n</i> = 2	14.70 <i>n</i> = 1
2	a	50.4 ± 45	51.0 ± 46	43.0 ± 39	0.92 ± 0.4	0.89 ± 0.3	0.96 ± 0.4	9.29 <i>n</i> = 1	8.80 ± 6.0 <i>n</i> = 2	20.65 ± 2.0 <i>n</i> = 2
3	a	21.8 ± 45	8.6 ± 57	60.2 ± 76	1.99 ± 1.4	1.40 ± 1.0	1.05 ± 1.2	32.3 ± 23.8 <i>n</i> = 3	15.30 ± 8.8 <i>n</i> = 3	14.97 ± 9.7 <i>n</i> = 2
4	a	32.1 ± 68	17.2 ± 49	6.3 ± 38	0.91 ± 0.9	1.07 ± 0.8	1.51 ± 1.2	11.51 ± 3.4	37.03 ± 15.1 <i>n</i> =	34.84 ± 13.5 <i>n</i> =
	b	24.1 ± 51	176.5 ± 57	131.2 ± 53	1.22 ± 0.8	1.18 ± 0.8	0.64 ± 0.4	18.52 ± 4.0 <i>n</i> = 2	29.66 ± 9.8 <i>n</i> = 3	16.10 ± 3.3 <i>n</i> = 3
	c	141.5 ± 34	132.9 ± 34	154.7 ± 40	0.92 ± 0.4	1.05 ± 0.6	1.32 ± 1.2	30.69 <i>n</i> = 1	39.66 ± 9.8 <i>n</i> = 2	30.96 ± 1.9 <i>n</i> = 2
5	a	27.5 ± 40	25.8 ± 57	22.9 ± 44	0.67 ± 0.4	0.85 ± 0.6	1.04 ± 0.5	–	17.77 ± 7.4 <i>n</i> = 2	12.60 <i>n</i> = 1
	b	14.9 ± 74	26.4 ± 52	36.7 ± 50	1.21 ± 0.8	0.98 ± 0.9	0.89 ± 0.6	–	–	24.22 <i>n</i> = 1
6	a	4.6 ± 45	2.9 ± 34	2.9 ± 38	1.13 ± 0.8	1.18 ± 0.8	1.05 ± 0.5	23.20 <i>n</i> = 1	25.23 ± 0.6 <i>n</i> = 2	27.20 ± 8.5 <i>n</i> = 3
	b	68.8 ± 63	59.0 ± 57	53.3 ± 62	0.53 ± 0.4	0.81 ± 0.6	1.35 ± 1.0	14.28 <i>n</i> = 1	7.86 <i>n</i> = 1	31.90 ± 5.2 <i>n</i> = 2

$$\frac{\partial U}{\partial t} + U \frac{\partial U}{\partial x} + V \frac{\partial U}{\partial y} = -\frac{1}{\rho} \frac{\partial P}{\partial x} + \nu \frac{\partial^2 U}{\partial x^2} + \nu \frac{\partial^2 U}{\partial y^2}$$

$$\frac{\partial V}{\partial t} + U \frac{\partial V}{\partial x} + V \frac{\partial V}{\partial y} = -\frac{1}{\rho} \frac{\partial P}{\partial y} + \nu \frac{\partial^2 V}{\partial x^2} + \nu \frac{\partial^2 V}{\partial y^2}$$

These equations were combined using the definition of vorticity (ω):

$$\omega = \frac{\partial U}{\partial y} - \frac{\partial V}{\partial x}$$

to eliminate the pressure variable:

$$\frac{\partial \omega}{\partial t} + U \frac{\partial \omega}{\partial x} + V \frac{\partial \omega}{\partial y} = +\nu \frac{\partial^2 \omega}{\partial x^2} + \nu \frac{\partial^2 \omega}{\partial y^2} \quad (1)$$

The incompressibility condition:

$$\frac{\partial U}{\partial x} + \frac{\partial V}{\partial y} = 0$$

implies that the velocity field could be written as a stream function (ψ):

$$U = \frac{\partial \psi}{\partial y}, \quad V = -\frac{\partial \psi}{\partial x} \quad (2)$$

In these equations, U and V are velocity components in the x and y directions, respectively, P is pressure, ρ is density and ν is molecular kinematic viscosity. By the definition of vorticity, an equation for the stream function was obtained:

$$\frac{\partial^2 \psi}{\partial x^2} + \frac{\partial^2 \psi}{\partial y^2} = \omega \quad (3)$$

The boundary conditions for ψ were specified on the ‘far away’ borders of a rectangular box to give a uniform velocity field. The boundary conditions for ω were obtained from the velocity field and the prescribed velocity of the objects within the flow. In this case, the large cylinder was stationary [U, V] = [0,0] and the small cylinder had a prescribed velocity [U_s, V_s] (Roache, 1972). The gradients of velocity components at the surface of the two cylinders were calculated, and vorticity on the surfaces was obtained. This was the source for vorticity at the surface of the cylinders that was then advected downstream by the non-linear terms of equation (1).

A time-stepping or iterative method was used to solve the equations. First, given an initial field of ω , ψ was solved from equation (3). Then U and V were obtained from equation (2). Finally, equation (1) was solved for the updated ω

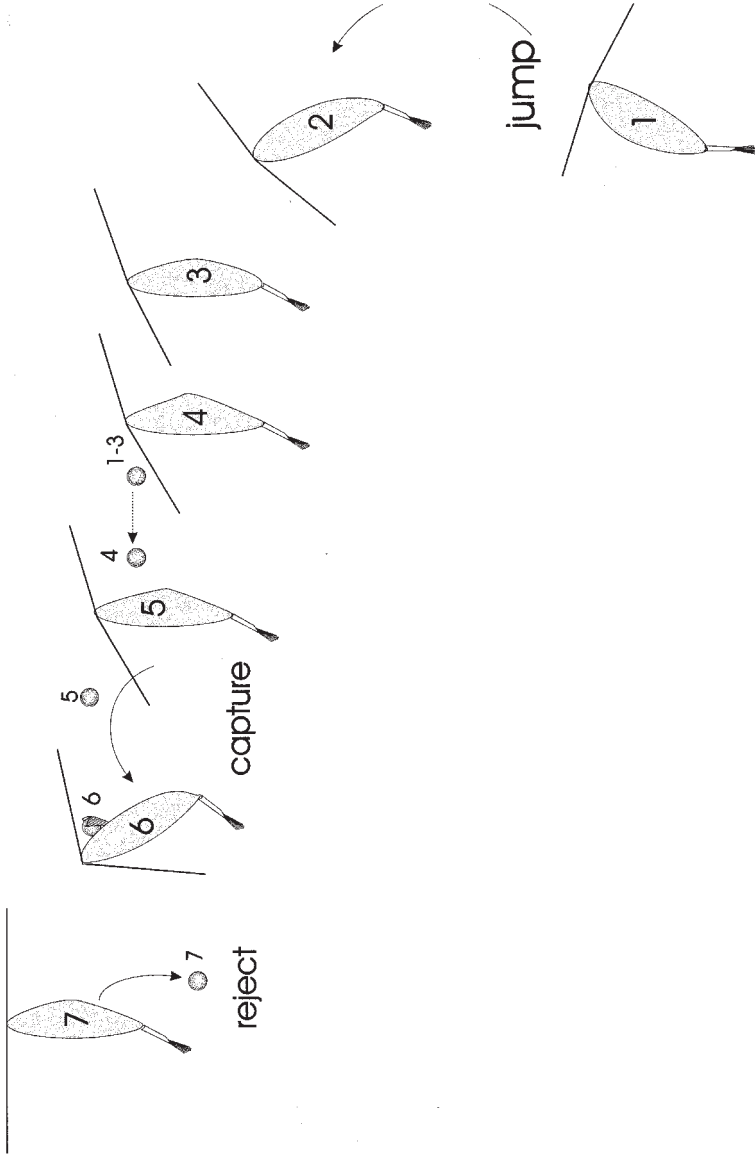


Fig. 2. Schematic drawing of the sequence of events leading to *D. sicilis* capturing an inert polystyrene bead. Numbers coordinate sequential events. (Copepod cephalothorax length = 1.2 mm, bead diameter = 50 μ m.)

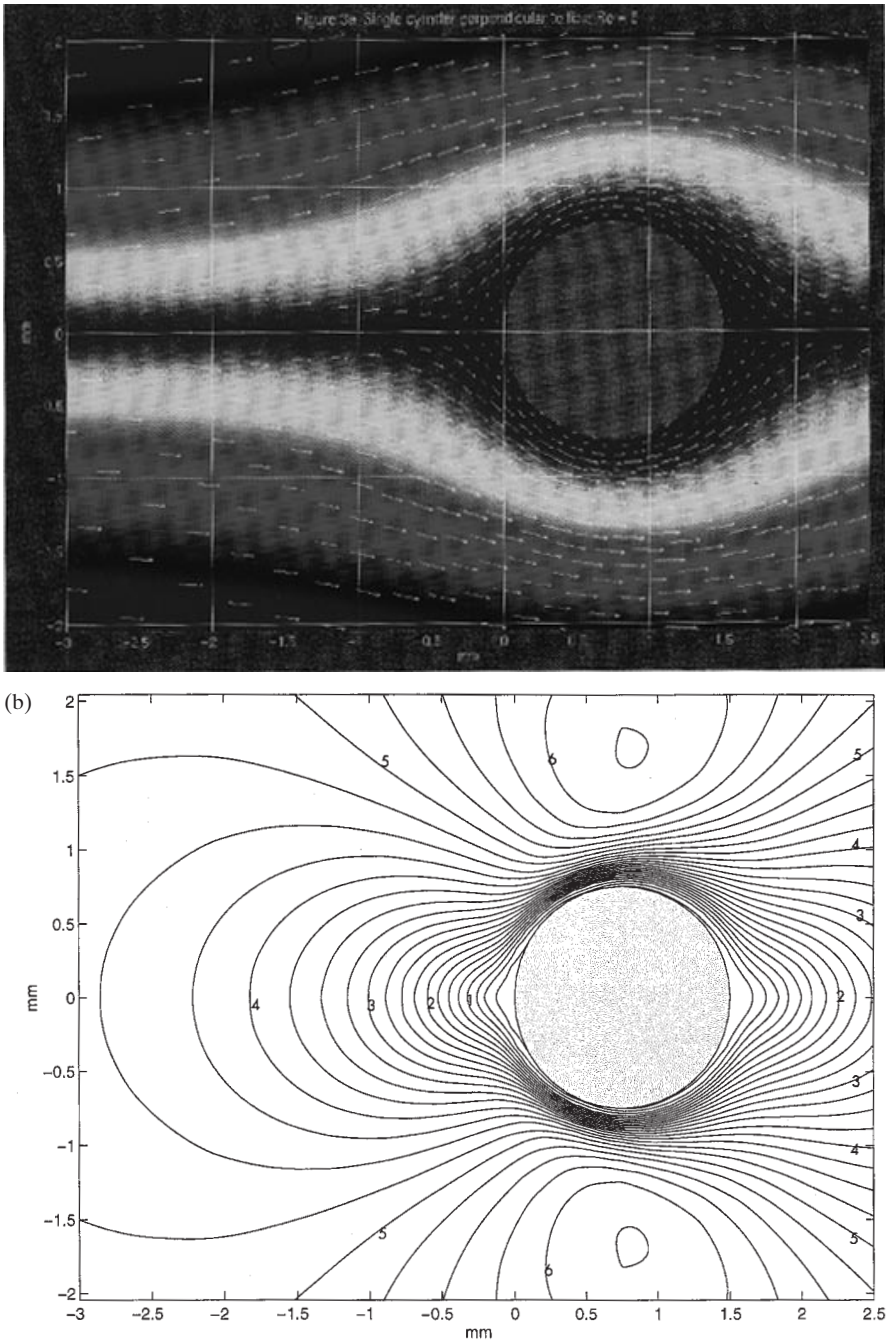


Fig. 3. Model predictions for a single cylinder oriented perpendicular to the flow. (a) Fluid streamlines around a single cylinder. Arrows represent fluid velocity vectors [circled vector is scaled to main-stream velocity (U) of 5 mm s^{-1}]. (b) Speed isolines around a single cylinder. Isolines are scaled to $U = 5 \text{ mm s}^{-1}$ and spaced at 0.25 mm s^{-1} intervals.

given the new U , V and ψ . The cycle was repeated until steady state (i.e. the variables did not change through a loop). This was a time-consuming method, because near Re of 5, perturbations and flow separations tend to grow, and convergence is slow. The field equations (1), (2) and (3) were solved on linear triangular finite elements with standard Galerkin functions (Burnett, 1987).

For the simulation of the physical interactions between a moving copepod and a non-moving prey item, we used a Re of 5 ($Re = l U \nu^{-1}$), which is in the range of Re experienced by adult *D.sicilis* when swimming and feeding. The length scale used for the model was the diameter of the large cylinder ($l = D$) = 1.5 mm, kinematic viscosity (ν) = 0.015 cm² s⁻¹ and main stream fluid velocity (U) = 5 mm s⁻¹. The model was first run for a small to large cylinder diameter ratio of 1:10 ($d:D$), and then for a length ratio of 1:3, because these values are in the range of typical copepod prey:predator body length ratios (Landry and Fagerness, 1988). These length scales provide a range for the numerical model that is realistic in terms of interactions between moving copepods and prey which have the ability to escape. Also, if flow field effects were not seen at these length scales, then they would not be expected at smaller length scales.

The model was first run for the large cylinder only (Figure 4). The small cylinder was then allowed to approach to the position where $x = -4d$, $y = 2d$, and then to the position where $x = -2d$, $y = 2d$ from the 'leading edge' of the large cylinder (Figures 5 and 6). In this manner, we simulated the important case of one object moving with the flow toward the other stationary object. Stated in the other relative coordinate system, we simulated the case of a larger moving object (the copepod) approaching a smaller stationary object (the prey item) which is deflected by the 'bow wake' of the former.

Results

Copepod behavior

The typical behavior of the copepod prior to an attack on a bead was characterized by bouts of slow swimming (1–2 mm s⁻¹) while creating a feeding current, punctuated by short, high-velocity jumps (12–26 mm s⁻¹). Immediately before an attack, the copepod jumped in the direction of the bead, then swam slowly toward the bead for a few seconds. As the copepod neared, the bead was displaced away from the approaching animal, rather than being entrained toward the copepod in the feeding current. Beads were displaced at velocities ranging from 0.5 to 1.2 mm s⁻¹. After swimming to within approximately a body length, the copepod attacked the bead by jumping toward it and capturing it. A typical sequence of behaviors associated with an attack on a bead is shown in Figure 3. In most cases, the copepod attacked the bead by jumping under the bead and capturing it, presumably with an extended feeding appendage. In some cases, the extended appendage could be seen capturing the bead, and in a few cases the copepod entrained the bead in its feeding current after jumping under the bead. Attack behavior was initiated within 0.25 s of bead movement. Attack behavior was not observed when copepods were feeding on single *C.reflexa* cells, but was frequently seen when copepods encountered beads. All beads were rejected after capture.

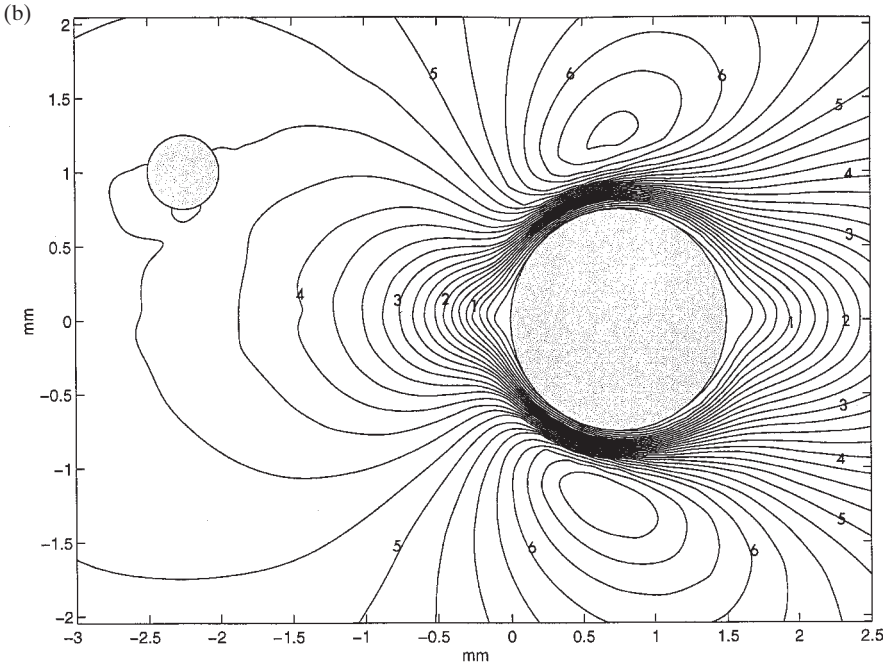
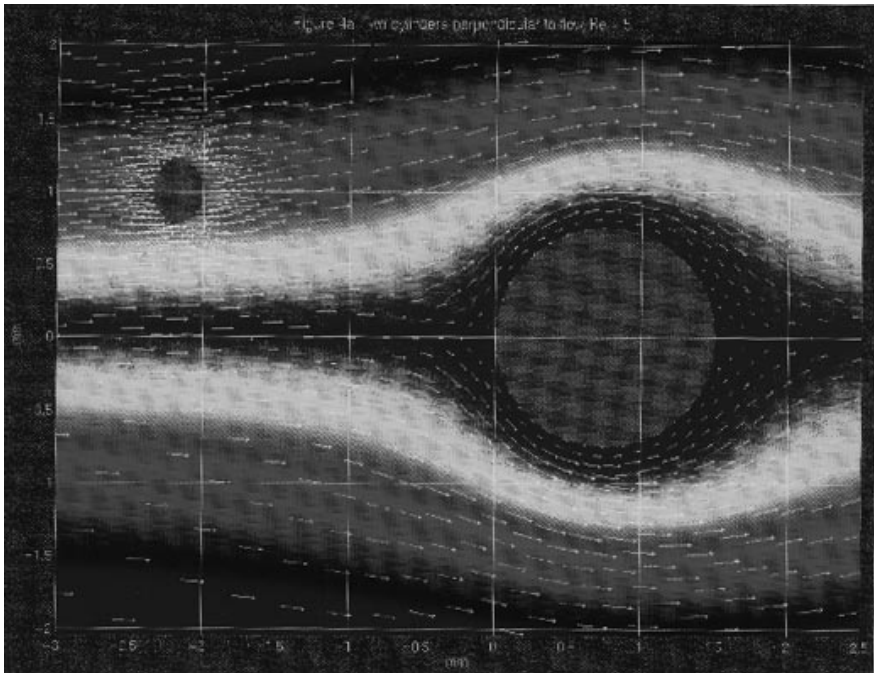


Fig. 4. Model predictions for two cylinders oriented perpendicular to the flow. Horizontal separation distance is $4d$ from the leading edge of the cylinders and vertical separation distance is $2d$. (a) Fluid streamlines. Arrows represent fluid velocity vectors [circled vector is scaled to mainstream velocity (U) of 5 mm s^{-1}]. (b) Speed isolines. Isolines are scaled to $U = 5 \text{ mm s}^{-1}$ and spaced at 0.25 mm s^{-1} intervals.

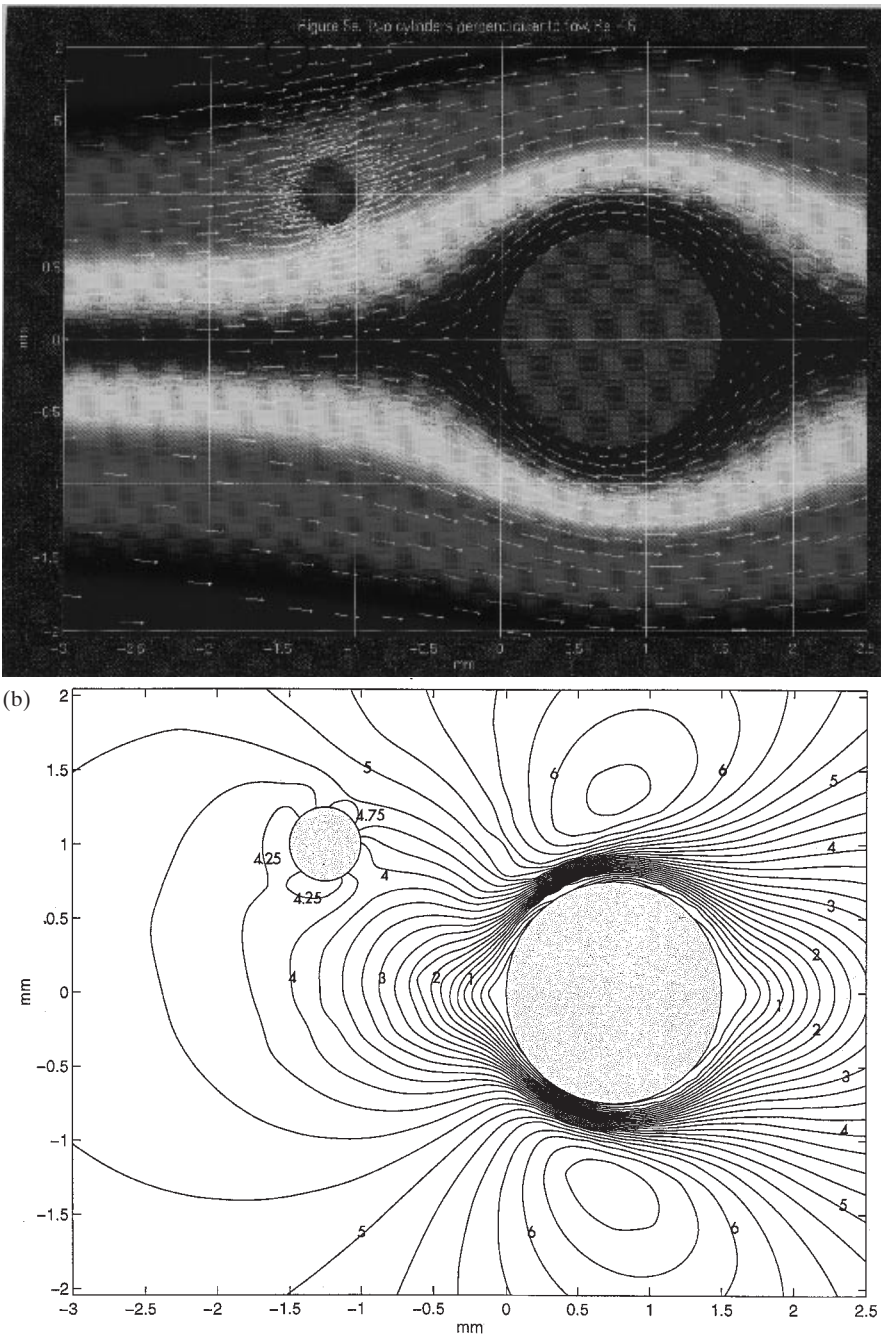


Fig. 5. Model predictions for two cylinders oriented perpendicular to the flow. Horizontal separation distance is $2d$ from the leading edge of the cylinders and vertical separation distance is $2d$. **(a)** Fluid streamlines. Arrows represent fluid velocity vectors [circled vector is scaled to mainstream velocity (U) of 5 mm s^{-1}]. **(b)** Speed isolines. Isolines are scaled to $U = 5 \text{ mm s}^{-1}$ and spaced at 0.25 mm s^{-1} intervals.

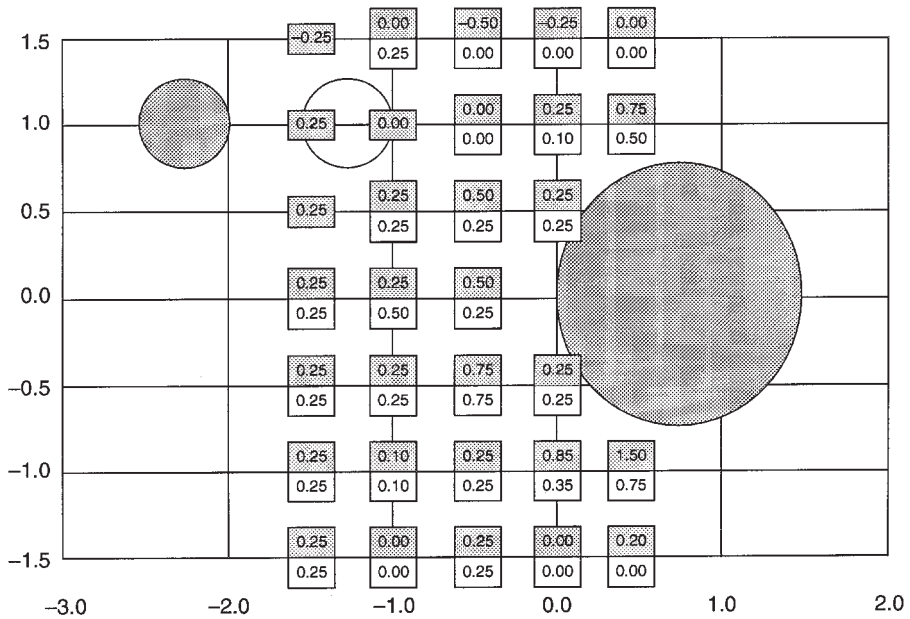


Fig. 6. Model predictions for absolute velocity fluctuations of fluid around two cylinders oriented perpendicular to a 5 mm s^{-1} flow. The shaded boxes correspond to the differences in velocity between the single-cylinder case (Figure 3b) and the case where the small cylinder is located at $4d$ (i.e. 2 mm) from the leading edge of the large cylinder (Figure 4b). The unshaded boxes correspond to the differences in velocity between the single-cylinder case and the case where the small cylinder is located at $2d$ (i.e. 1 mm) from the leading edge of the large cylinder (Figure 5b).

At a concentration of 4 beads ml^{-1} , the number of observed attacks on beads ranged from 0 to 7 per 30–60 min observation period for each of 11 copepods (mean capture rate = 4.5 beads h^{-1} , $\text{SD} = 1.5 \text{ beads h}^{-1}$). From these data, we can estimate clearance rates of beads at $\sim 27 \text{ ml copepod}^{-1} \text{ day}^{-1}$. Video images showed that the beads were not homogeneously distributed throughout the volume of the filming vessel and, as is expected when food particles are not uniformly distributed, capture rates varied over time.

Many captures occurred when copepods were close to walls, which may influence fluid dynamics between objects moving relative to each other. We therefore only selected events for quantitative behavioral analyses that occurred $>1 \text{ cm}$ from filming vessel surfaces, and in which the copepod and the bead were in focus and in view for 10 s prior to the attack. Ten capture events involving six copepods were selected for detailed analyses.

Table I shows the time interval between the last jump and the capture event; the orientation of the copepod to the bead immediately after the last jump and the orientation just prior to the attack jump; attack distances; and the distance of the bead from the copepod when the bead first began to move away from the approaching copepod. Distances are conservative estimates because they are

calculated from two-dimensional data. This is especially true when the copepod was oriented in a more dorsal or ventral view.

A subset of the observation interval was then partitioned into three 3 s intervals (total of continuous 9 s observed prior to an attack) (Table III). We wanted to determine whether specific behaviors changed in the interval just before an attack (i.e. velocities decreased or increased, or trajectories became smaller or larger, or jumps were directed upward or downward). When copepod velocity and trajectory during the 3 s interval immediately before an attack were compared with behavior during 3 s intervals beginning 9 and 6 s before an attack, no quantitative differences could be detected (paired *t*-test). The jumps also could not be shown to be biased in any direction (runs test; Dixon and Massey, 1951). Consequently, the movements of the copepod prior to the slow swim toward the bead before an attack could not be shown to be directed to the bead, and there was no other evidence that the copepods detected the presence and location of the beads until immediately before an attack.

There were, however, consistent copepod–bead interactions that preceded each attack: (i) in every case, beads were displaced away from the moving copepod immediately prior to an attack; and (ii) in nine of the 10 attacks, copepods initiated the attack only after the approach angle approximated 90° (Figure 1 and Table I). Because the bead was always anterior–dorsal to the copepod at the time of the attack jump, and because it moved away from the copepod before being captured, the detection of these large inert particles did not involve the feeding current. A feeding current was, however, generated by the copepod during all bouts of slow swimming (i.e. phytoplankton cells were entrained in flow toward the mouthparts).

Model results

The numerical model showed no detectable effect of the small cylinder on the flow field surrounding the large cylinder when length-scale ratios of 1:10 were tested. Therefore, only the results of the model runs using a length-scale ratio of 1:3 are reported here. At a length-scale ratio of 1:3, the numerical model revealed that the smaller cylinder evoked a fluctuation in the velocity field around the larger cylinder, as the boundary layers and wake flows of the two objects interacted. Figures 3, 4 and 5 show fluid velocities, streamlines and fluid speed for $Re = 5$. The velocities and streamlines are relative to the moving large cylinder, which is portrayed ‘at rest’ in the figures. This is an identical scenario to that which portrays the larger cylinder moving toward the smaller. Streamline color is consistent between figures, and fluid velocity is represented by the accompanying vectors. Speed isolines connect points where the magnitudes of velocity are equal. Figure 3 shows the model results for flow around a single cylinder (diameter = D). Note that streamlines and speed isolines are symmetrical above and below the cylinder, and a stagnation point is located at the center of the ‘leading edge’. Velocity vectors and an increase in streamline spacing show that fluid slowed as it approached the cylinder. As fluid was accelerated around the cylinder, spacing between streamlines decreased. These results are consistent with

predictions and empirical observations of flow geometry around circular cylinders at low Re (e.g. Batchelor, 1967; Van Dyke, 1981; Vogel, 1994).

Flow field geometry and fluid speeds were first compared between the single large cylinder case and the case where the leading edge of the small cylinder (diameter = d) was located at $x = -4d$, $y = 2d$ (i.e. $x = -2$ mm, $y = 1$ mm for a 5 mm s^{-1} flow at $Re = 5$) (Figures 3 and 4). When the smaller cylinder was embedded in the flow, as the larger cylinder approached, the influence of the small cylinder was manifested as a deformation of streamlines and an increase in fluid velocity in the region between the cylinders, compared to the same region of the flow field when the small cylinder was absent (Figures 3a and 4a). Streamlines were compressed and shifted vertically (i.e. in the direction of the small cylinder). When the velocities at 0.5 mm intervals directly in front of the cylinder are compared between cases, e.g. at $x = -0.5$, $y = 0.0$ (Figures 3b and 4b), fluid speed increased from 35% of mainstream velocity for the single-cylinder case to ~45% of mainstream velocity when the small cylinder was present. Fluid speed at $x = -1.0$, $y = 0.0$ increased from 60% of mainstream velocity for the single large cylinder case to 70% for the case when the small cylinder was present. The maximum speed of the fluid moving around the large cylinder increased from a maximum of 125% for the single large cylinder case to 135% of mainstream velocity when the small cylinder was present.

When the separation distance between the cylinders was decreased and the small cylinder was moved to $x = -2d$, $y = 2d$ (e.g. $x = -1$ mm, $y = 1$ mm for a 5 mm s^{-1} flow at $Re = 5$; Figure 5), flow field geometry and velocity distribution again were altered. Streamline compression in the region between the two cylinders relaxed (Figure 5a), and the fluid speed in the region directly in front of the large cylinder ($x = -0.5$, $y = 0.0$) decreased from 45% for the larger separation distance (Figure 4b) to ~40% of mainstream velocity for the smaller separation distance case (Figure 5b). Fluid speed at $x = -1.0$, $y = 0.0$ also decreased compared to the larger separation distance case from 70% to 65% of mainstream velocity. The flow field above the large cylinder also changed as separation distance decreased. The maximum velocity region decreased to 130% of mainstream velocity and extended farther from the cylinder than in the case of the large separation distance (Figures 4b and 5b). Speed isolines also shifted toward the upstream direction.

Figure 6 shows the relative changes in velocity assuming a mainstream flow of 5 mm s^{-1} at $Re = 5$ for the three cases. The baseline or reference velocity for the changes is the fluid velocity at the corresponding location for the single-cylinder case (Figure 3b). The largest absolute changes in velocity, relative to the single-cylinder case, are seen within ~0.5 mm of the surface of the large cylinder. Figure 6 also shows the magnitude of speed fluctuations as the separation distance between the large and small cylinders decreases. The largest fluctuations (0.5 and 0.75 mm s^{-1}) are seen in a region above the smaller cylinder (at $x = -0.5$, $y = 1.5$) and in a region below and upstream from the large cylinder (between $x = 0.0$, $y = -1.0$ and $x = 0.5$, $y = -1.0$).

The small cylinder is given a prescribed speed in the model that matches the local streamline speed. Figures 4b and 5b show speed contours intercepting the

surface of the small cylinder, which indicates that the speed of the small cylinder became mismatched with the local streamline speed. This was due to the incompressible volume of the small cylinder crossing streamlines and distorting velocity contours associated with the large cylinder. Although the individual contours for the relative speed of the small cylinder are represented graphically as intercepting the cylinder, the average fluid speed surrounding the cylinder may not match its actual speed. For example, in Figure 5b, the top of the small cylinder pushes water a little faster than the bottom, and the 4.75 mm s^{-1} contour curves toward the cylinder. In other words, the bottom of the small cylinder ‘trips up’ in the lower velocity fluid. In this case, the prescribed relative speed of the small cylinder was 4.4873 mm s^{-1} , but the numerically modeled average was 4.3 mm s^{-1} , resulting in a mismatch of $\sim 0.2 \text{ mm s}^{-1}$ or $\sim 5\%$ of the local velocity. The net result of this disturbance on the velocity field was a downstream perturbation near the large cylinder. This downstream perturbation would be seen as temporal changes in velocity as the small cylinder approached in the boundary layer flow.

In summary, we found that as separation distances between the two objects decreased, (i) velocity fluctuations arose in the region between and above the two objects, and (ii) the spatial distribution of the velocity field changed temporally. The numerical model examined the simple case of two cylinders with diameter ratios of 3:1. The model results suggest that in the more complicated case of a complex shape (the copepod and its first antennae) and a smaller sphere (the polystyrene bead) functioning at similar Re , flow fields may also be distorted, although the magnitude of velocity fluctuations would probably be smaller, and the geometry of the flow fields would most likely differ.

Discussion

Perception of distant objects by calanoid copepods using mechanoreception has been documented by the ability of freely swimming copepods to detect and capture moving prey located outside the influence of the feeding current (Gauld, 1966; Williamson and Butler, 1986; Jonsson and Tiselius, 1990) and by tethered copepods capturing polystyrene beads in the feeding current (Vanderploeg *et al.*, 1990). It is not difficult to understand that a motile particle such as a nauplius or a ciliated larva creates a detectable hydrodynamic signal, because these living particles move and displace fluid (Yen and Fields, 1992; Gallagher, 1993). However, the sensory mechanisms that calanoid copepods use to detect inert particles (i.e. those that do not move independently and have no odor) are not well understood, because the inert particles must first be displaced by an external force before a hydrodynamic disturbance is produced. Calanoids may detect streamline deformations around large obstacles in their paths (Haury *et al.*, 1980) and, in the present study, were seen actively to avoid the walls of the filming vessel.

Because the attacked particles in this study are inert, the stimulus detected by the copepod must be a hydrodynamic signal, rather than a chemical stimulus. For foraging diaptomids, mechanoreception must therefore play an integral part in the detection of large, prey-sized, non-moving particles. The concept that copepods

have the ability to detect and capture non-motile particles outside the feeding current is novel, and adds yet another dimension to the repertoire of feeding behaviors that allow copepods to survive in a highly variable environment.

The biophysics of prey detection is complicated at the *Re* characteristic of the fluid environment where copepods feed and move about (*Re* 0.01–100 for a 1 mm copepod). An acoustic pressure differential (far-field disturbance or sound wave) and fluid displacement (near-field disturbance) are both associated with moving particles (Kalmijn, 1988). Légier-Visser *et al.* (1986) suggested that copepods detect a non-acoustic pressure disturbance in the flow field of the feeding current as particles are entrained toward the first antennae (A1). Although a pressure differential is associated with a change in streamline velocity, copepods do not have the physiological ability to detect a pressure gradient.

The sensory organs used to detect pressure gradients require a ‘pressure-to-motion converter’ (e.g. a transducer such as the swim bladder of a fish) (von Frisch, 1938). Crustaceans lack such a transducer and rely instead on the fluid displacement component of the signal as the mediator of responses to hydrodynamic stimuli (Tautz, 1979). While a pressure disturbance accompanies the fluid deformation associated with an obstacle embedded in the flow, the signal detected by the copepod in this case would be the change in velocity of the fluid around its sensory structures.

Calanoid first antennae are morphologically and physiologically well suited as detectors of velocity fluctuations. The A1 are long cylindrical structures that have hair-like setae arranged in rows along their axes. The mechanoreceptive setae in this array contain the terminal segments of mechanosensory neurons (Strickler and Bal, 1973; Barrientos, 1980; Gresty *et al.*, 1993; Weatherby *et al.*, 1994). A mechanoreceptive seta is stimulated when the fluid velocity around the seta changes and the resultant shear displaces the hair, distorting the membranes of mechanosensitive dendrites inserted into its base (French, 1988). Transduction of the stimulus occurs when the membrane of a sensory neuron is sufficiently deformed to open ion channels and create a potential across the cell membrane (French, 1988; Corey and García-Añoveros, 1996). These displacements do not need to be large in magnitude: electrophysiological studies of antennal responses to a high-frequency dipole source confirm that setae are sensitive to displacements as small as 10 nm (Lenz and Yen, 1993).

When a stationary particle has a density different from the surrounding fluid, its momentum will cause it to be accelerated and ‘cross’ streamlines associated with the wake and boundary layer of a larger approaching object, causing a large disturbance. However, because algal cells and the inert polystyrene beads have a density very close to water, their effect on the boundary layer should be more subtle and should be due primarily to the solid body motion of the particle ‘spanning’ streamlines. We hypothesize that the disturbance from the bead is detected by the flexible mechanoreceptive setae on the A1 as they are displaced by the flow shear created by the copepod’s body wake flow and boundary layer, plus the additional deformation when an obstacle is present. Simply put, the mechanoreceptive setae on the A1 are displaced as the velocity gradient around the A1 is altered by the obstacle.

The extent and location of the fluid deformation predicted by the model depend on the orientation of the two objects to each other and their relative motion and size. If the physical phenomena described in the model hold for swimming copepods foraging on large non-motile prey, then the orientation of sensory structures and the swimming velocity of the copepod should be critical to the predator's ability to detect its prey by this physical mechanism. The mechanism would not be available to a 'hovering' copepod.

When we examine three-dimensional reconstruction of confocal images, we find that the sensory hairs (setae) of A1 of *D.sicilis* are oriented in an anterior–dorsal direction (Figure 7a and b). The setae were tentatively identified as mechanoreceptors because of their characteristic morphology and the presence of an articulated socket (Figure 7a), although they may be dually functional and have some chemoreceptive function as well (Tautz, 1979; Kurbjewit and Buchholz, 1991; Weatherby *et al.*, 1994). The shorter putative mechanoreceptors (~100 μm in length) are located along the anterior–dorsal edge of the A1 and the longer putative mechanoreceptors (~300 μm in length) are located on the anterior edge of the A1 (Figure 7b). Video images show that the approach angle of the copepod prior to an attack swings from ~120 to 90° as the copepod approaches the bead. Therefore, as *D.sicilis* moves toward a bead that is ultimately captured, the sensilla projecting ahead of the animal and lying parallel to and at an angle to its body axis transcribe an arc relative to the bead. This is because the copepod swims with its ventral side up (Figure 7b).

Model results showed that fluctuating flow field effects were pronounced in the region between the two objects as separation distances decreased (Figure 6). An orientation angle between 120 and 90° would place the putative mechanoreceptors in this region of the boundary layer as the copepod neared the bead. Boundary layers around many freely swimming calanoids are most pronounced in this anterior–dorsal region (i.e. the low-velocity region, compared to freestream velocity, is 'thicker' here) (Tiselius and Jonsson, 1990; Bundy and Paffenhöfer, 1996). The geometry of the boundary layer is dependent on swimming velocity and the orientation of the moving copepod (Bundy and Paffenhöfer, 1996).

The behavioral advantage of detecting and capturing motile prey without utilizing the feeding current may lie in the element of surprise. Prey react to velocity gradients (shear and vorticity) in the copepod's feeding current (Williamson, 1987; Jonsson and Tiselius, 1990; Fields and Yen, 1997). Many nauplii and other microzooplankton do not move until disturbed (Williamson and Vanderploeg, 1988; Paffenhöfer *et al.*, 1996), and some cladocerans use a 'dead man' strategy to avoid capture once they are attacked (Kerfoot *et al.*, 1978). Tiselius and Jonsson (1990) noticed that copepods could approach closer to prey that were located in the anterior–dorsal region of the flow field where feeding current disturbances were lower. Clearance rates of omnivorous calanoids on prey that tend to escape from feeding current flow fields should be enhanced by this behavior.

Omnivorous copepods would also benefit from this feeding mode when they are feeding on mixed populations of motile and non-motile prey. The generation of a feeding current while swimming slowly is an efficient tool for feeding on

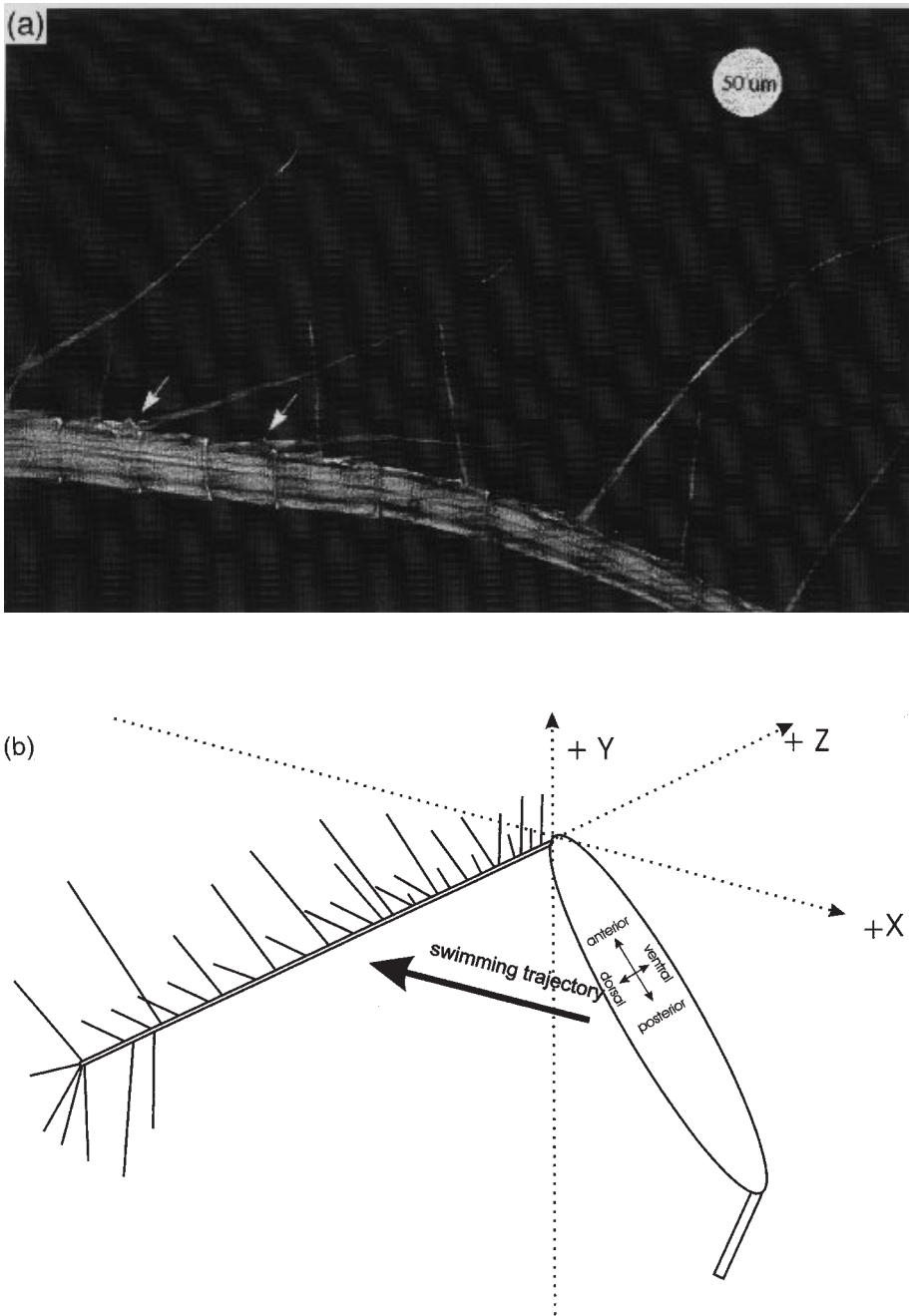


Fig. 7. *Diaptomus sicilis* first antenna (A1). (a) Laser scanning confocal micrograph of the dorsal view of the right A1 of *D. sicilis*. The long thin setae are putative mechanoreceptive sensilla. Arrows indicate the articulated base of sensilla. A 50-µm-diameter 'bead' is drawn in for scale. (b) Schematic drawing showing copepod swimming trajectory and orientation of A1 and setae are approximately proportional to copepod body length.

non-motile prey or on prey with limited escape capabilities. However, motile prey with well-developed escape capabilities may be stimulated to escape by the feeding current disturbance (Fields and Yen, 1997). An omnivore such as *D.sicilis* could utilize both types of prey by combining bouts of slow swimming with intermittent hops. This behavior was observed in the present study.

Large diatoms, such as *Melosira italica*, which dominate the water column during spring and the deep chlorophyll layer during summer (Fahnenstiel and Scavia, 1987), are important components of the diet of *D.sicilis* (e.g. Vanderploeg *et al.*, 1988). It may be that the repeated hopping and turning behavior exhibited by *D.sicilis* (Ramcharan and Sprules, 1991; present study) allows this copepod to utilize the foraging mechanism described here to capture large non-motile phytoplankton cells that may otherwise have remained undetected. Note that the clearance rates on beads reported here for *D.sicilis* fall within the range (25–42 ml day⁻¹ copepod⁻¹) reported for this species feeding on large diatoms (Vanderploeg *et al.*, 1988). Cyclopoid copepods, such as *Oithona spinirostris*, do not create feeding currents (Landry and Fagerness, 1988), yet graze efficiently on large, non-motile cells. Cyclopoids move in hops and jumps, as well as in slow swimming mode (Shuvayev, 1978; Williamson, 1981; Uchima and Murano, 1988; Paffenhöfer *et al.*, 1996). The feeding mechanism described here may also explain how cyclopoids are able to detect and capture large non-motile phytoplankton.

Predator–prey interactions are constrained by behavior and by ambient fluid motions. To understand fully the mechanisms governing prey detection and capture, it is important that animals are observed as they move about freely. We must also have information on the sensitivity of the sensory structures that receive the signals from potential prey. Because the shapes of copepods and their prey are complex, and because they move in non-linear and unpredictable patterns, a numerical model cannot precisely replicate predator–prey interactions in nature. However, the model developed in this study shows us that flow field distortion between two objects moving relative to each other can be quantified and predicted for a simple test case using length scales and a Reynolds number similar to those in the visual observations. This investigation into the physics of particle detection in a quiescent fluid has enhanced our understanding of the physical, behavioral and physiological processes that may control predator–prey interactions of calanoid copepods. We see here that mechanoreception alone may be used to detect remotely located non-motile prey.

Preliminary studies of freely swimming *Diaptomus* spp., conducted in this laboratory, also showed that inert beads can be detected and captured in the feeding current flow. Future studies will evaluate the relative importance of capturing particles within and outside the feeding current, and will investigate the influence of small-scale ambient water motion on behavior and on the ability of calanoids to capture inert particles. These variables must be considered together before we can better understand the role of feeding behavior in controlling community structure in aquatic systems.

Acknowledgements

This study was supported by the Great Lakes Environmental Research Laboratory (GLERL), and with funding from a postdoctoral award to M.H.B. from the National Research Council Resident Research Associateship Program. We thank S.Ruberg for his help with the design and implementation of the camera positioning software, and G.-A.Paffenhöfer for his help and advice on the set-up of the camera positioning hardware. Two anonymous reviewers provided valuable suggestions and comments that improved the manuscript. We also thank the staff and ship crew at GLERL's Lake Michigan Field Station for help with zooplankton collection. This paper is GLERL contribution no. 1063.

References

- Alcaraz,M., Paffenhöfer,G.-A. and Strickler,J.R. (1980) Catching the algae: a first account of visual observations on filter feeding calanoids. In Kerfoot,W.C. (ed.), *The Evolution and Ecology of Zooplankton Communities*. University Press of New England, Hanover, NH, pp. 241–248.
- Andrews,J.C. (1983) Deformation of the active space in the low Reynolds number feeding current of calanoid copepods. *Can. J. Fish. Aquat. Sci.*, **40**, 1293–1302.
- Barrientos,Y.C. (1980) Ultrastructure of sensory units on the first antennae of calanoid copepods. MSc Thesis, University of Ottawa, Ottawa, Canada, pp. 1–81.
- Batchelor,G.K. (1967) *An Introduction to Fluid Dynamics*. Cambridge University Press, London, 615 pp.
- Bundy,M.H. and Paffenhöfer,G.-A. (1993) Innervation of copepod antennules investigated using laser scanning confocal microscopy. *Mar. Ecol. Prog. Ser.*, **102**, 1–14.
- Bundy,M.H. and Paffenhöfer,G.-A. (1996) Analysis of flow fields associated with freely swimming calanoid copepods. *Mar. Ecol. Prog. Ser.*, **133**, 99–113.
- Burnett,D.S. (1987) *Finite Element Analysis*. Addison-Wesley, Reading, MA, 844 pp.
- Butler,N.M., Suttle,C.A. and Neill,W.E. (1989) Discrimination by freshwater zooplankton between single algal cells differing in nutritional status. *Oecologia (Berlin)*, **78**, 368–372.
- Cain,M.L. (1989) The analysis of angular data in ecological field studies. *Ecology*, **70**, 1540–1543.
- Corey,D.P. and García-Añoveros,J. (1996) Mechanosensation and the DEG/ENaC ion channels. *Science*, **273**, 323–324.
- Cowles,T.J., Olson,R.J. and Chisholm,S.W. (1988) Food selection by copepods: discrimination on the basis of food quality. *Mar. Biol.*, **100**, 41–49.
- DeMott,W.R. and Watson,M.D. (1991) Remote detection of algae by copepods: responses to algal size, odors and motility. *J. Plankton Res.*, **13**, 1203–1222.
- Dixon,W.J. and Massey,F.J. (1951) *Introduction to Statistical Analysis*. McGraw-Hill, Inc., New York, 370 pp.
- Donaghay,P.L. and Small,I.F. (1979) Food selection capabilities of the estuarine copepod *Acartia clausii*. *Mar. Biol.*, **52**, 137–146.
- Fahnenstiel,G.L. and Scavia,D. (1987) Dynamics of Lake Michigan phytoplankton: recent changes in surface and deep communities. *Can. J. Fish. Aquat. Sci.*, **44**, 509–514.
- Fields,D.M. and Yen,J. (1997) Implications of the feeding current structure of *Eucheata rimana*, a carnivorous pelagic copepod, on the spatial orientation of their prey. *J. Plankton Res.*, **19**, 79–95.
- French,A.S. (1988) Transduction mechanisms of mechanosensilla. *Annu. Rev. Entomol.*, **33**, 39–58.
- Friedman,M.M. (1980) Comparative morphology and functional significance of copepod receptors and oral structures. *Am. Soc. Limnol. Oceanogr. Spec. Symp.*, **3**, 185–197.
- Gallager,S.M. (1993) Hydrodynamic disturbances produced by small zooplankton: case study for the veliger larva of a bivalve mollusc. *J. Plankton Res.*, **15**, 1277–1296.
- Gauld,D.T. (1966) Swimming and feeding of planktonic copepods. In Barnes,H. (ed.), *Some Contemporary Studies in Marine Science*. George Allen and Unwin, London.
- Gresty,K.A., Boxshall,G.A. and Nagasawa,K. (1993) Antennular sensors of the infective copepodid larva of the salmon louse, *Lepeophthierus salmonis* (Copepoda: Caligidae). In Boxshall,G.A. and Defaye,D. (eds), *Pathogens of Wild and Farmed Fish: Sea Lice*. Ellis Horwood, Chichester, pp. 83–98.
- Harvey,H.W. (1937) Note on selective feeding by *Calanus*. *J. Mar. Biol. Assoc. UK*, **22**, 97–100.
- Haury,L., Kenyon,D.E. and Brooks,J.R. (1980) Experimental evaluation of the avoidance reaction of *Calanus finmarchicus*. *J. Plankton Res.*, **2**, 187–202.

- Jonsson,P.R. and Tiselius,P. (1990) Feeding behavior, prey detection and capture efficiency of the copepod *Acartia tonsa* feeding on planktonic ciliates. *Mar. Ecol. Prog. Ser.*, **60**, 35–44.
- Kalmijn,Ad.J. (1988) Hydrodynamic and acoustic field detection. In Atema,J., Fay,R.R., Popper,A.N. and Tavolga,W.N. (eds), *Sensory Biology of Aquatic Organisms*. Springer-Verlag, New York, pp. 83–130.
- Kerfoot,W.C., Kellogg,D.L. and Strickler,J.R. (1978) Visual observations of live zooplankters: evasion, escape and chemical defenses. In Kerfoot,W.C. (ed.), *The Evolution and Ecology of Zooplankton Communities*. University Press of New England, Hanover, NH, pp. 10–27.
- Koehl,M.A.R. and Strickler,J.R. (1981) Copepod feeding currents: Food capture at low Reynolds number. *Limnol. Oceanogr.*, **26**, 1062–1073.
- Kurbjeweit,F. and Buchholz,C. (1991) Structures and suspected functions of antennular sensilla and pores of three Arctic copepods (*Calanus glacialis*, *Metridia longa*, *Paraeuheatia norvegica*). *Meeresforsch.*, **33**, 168–182.
- Landry,M.R. and Fagerness,V.L. (1988) Behavioral and morphological influences on predatory interactions among marine copepods. *Bull. Mar. Sci.*, **43**, 509–529.
- Légier-Visser,M., Mitchell,J.G., Okubo,A. and Fuhrman,J.A. (1986) Mechanoreception in calanoid copepods: a mechanism for prey detection. *Mar. Biol.*, **90**, 529–536.
- Lenz,P.H. and Yen,J. (1993) Distal setal mechanoreceptors of the first antennae of marine copepods. *Bull. Mar. Sci.*, **53**, 170–179.
- Paffenhöfer,G.-A. and Lewis,K.D. (1990) Perceptive performance and feeding behavior of calanoid copepods. *J. Plankton Res.*, **12**, 933–946.
- Paffenhöfer,G.-A., Strickler,J.R. and Alcaraz,M. (1982) Suspension-feeding by herbivorous calanoid copepods: a cinematographic study. *Mar. Biol.*, **67**, 193–199.
- Paffenhöfer,G.-A., Strickler,J.R., Lewis,K.D. and Richman,S. (1996) Motion behavior of nauplii and early copepodid stages of marine planktonic copepods. *J. Plankton Res.*, **9**, 1699–1715.
- Ramcharan,C.W. and Sprules,W.G. (1991) Predator-induced behavioral defense and its ecological consequences for two calanoid copepods. *Oecologia (Berlin)*, **86**, 276–286.
- Roache,P.J. (1972) *Computational Fluid Dynamics*. Hermosa, Albuquerque, NM, 446 pp.
- Shuvayev,D. (1978) Movement of some planktonic copepods. *Hydrobiol. J. (USSR)*, **14**, 32–36.
- Strickler,J.R. (1985) Feeding currents in calanoid copepods: Two new hypotheses. In Laverack,M.S. (ed.), *Physiological Adaptations of Marine Animals*. Society for Experimental Biology, UK, pp. 459–485.
- Strickler,J.R. and Bal,A.K. (1973) Setae of the first antennae of the copepod *Cyclops scutifer* (Sars): their structure and importance. *Proc. Natl Acad. Sci. USA*, **70**, 2656–2659.
- Tautz,J. (1979) Reception of particle oscillation in a medium—an unorthodox sensory capacity. *Naturwissenschaften*, **65**, 452–461.
- Tiselius,P. and Jonsson,P. (1990) Foraging behavior of six calanoid copepods: observation and hydrodynamic analysis. *Mar. Ecol. Prog. Ser.*, **66**, 23–33.
- Uchima,A.M. and Murano,M. (1988) Swimming behavior of the marine copepod *Oithona davisae*: internal control and search for environment. *Mar. Biol.*, **99**, 47–56.
- Van Dyke,M. (1981) *An Album of Fluid Motion*. The Parabolic Press, Stanford, CA, 176 pp.
- Vanderploeg,H.A. and Paffenhöfer,G.-A. (1985) Modes of algal capture by the freshwater copepod *Diaptomus sicilis* and their relation to food-size selection. *Limnol. Oceanogr.*, **30**, 871–885.
- Vanderploeg,H.A., Paffenhöfer,G.-A. and Liebig,J.R. (1988) *Diaptomus* vs. net phytoplankton: Effects of algal size and morphology on selectivity of a behaviorally flexible, omnivorous copepod. *Bull. Mar. Sci.*, **43**, 561–572.
- Vanderploeg,H.A., Paffenhöfer,G.-A. and Liebig,J.R. (1990) Concentration-variable interactions between calanoid copepods and particles of different food quality: Observations and hypotheses. In Hughes,R.N. (ed.), *Behavioral Mechanisms of Food Selection. NATO ASI Series G20*. Springer-Verlag, Berlin, Heidelberg.
- Vogel,S. (1994) *Life in Moving Fluids*. Princeton University Press, Princeton, NJ.
- von Frisch,K. (1938) The sense of hearing in fish. *Nature*, **141**, 8–11.
- Weatherby,T.M., Wong,K.K. and Lenz,P.H. (1994) Fine structure of the distal sensory setae on the first antennae of *Pleuromamma xiphias* Giesbrecht (Copepoda). *J. Crust. Biol.*, **14**, 670–685.
- Weiss,D.G., Keller,F., Gulden,J. and Maile,W. (1986) Towards a new classification of intracellular particle movements based on quantitative analyses. *Cell Motil. Cytoskel.*, **6**, 128–135.
- Williamson,C.E. (1981) Foraging and looping behavior of a freshwater copepod: Frequency changes in looping behavior at high and low prey densities. *Oecologia (Berlin)*, **50**, 332–336.
- Williamson,C.E. (1987) Predator-prey interactions between omnivorous diaptomid copepods and rotifers: The role of prey morphology and behavior. *Limnol. Oceanogr.*, **32**, 167–177.
- Williamson,C.E. and Butler,N.M. (1986) Predation on rotifers by the suspension-feeding calanoid copepod *Diaptomus pallidus*. *Limnol. Oceanogr.*, **31**, 393–402.

- Williamson,C.E. and Vanderploeg,H. (1988) Predatory suspension-feeding in *Diaptomus*: Prey defenses and the avoidance of cannibalism. *Bull. Mar. Sci.*, **43**, 561–572.
- Yen,J. and Fields,D.M. (1992) Escape responses of *Acartia hudsonica* (Copepoda) nauplii from the flow field of *Temora longicornis* (Copepoda). *Arch. Hydrobiol. Beih. Ergebn. Limnol.*, **36**, 123–134.

Received on November 24, 1997; accepted on June 23, 1998